Heated fiber optic distributed temperature sensing for measuring soil volumetric heat capacity and water content: A dual heat-pulse probe approach

Javier Benítez-Buelga,* Chadi Sayde, Leonor Rodríguez-Sinobas, John S. Selker

J. Benítez-Buelga and L. Rodríguez-Sinobas, Department of Rural Engineering, Technical University of Madrid, Av/Complutense sn, 28040, Madrid, Spain, and C. Sayde and J. S. Selker, Department of Biological & Ecological Engineering, Oregon State University, Corvallis, OR, USA.

*Corresponding author (javier.benitez@upm.es)

Abstract

Implementation of the Dual Probe Heat Pulse (DPHP) theory for measurement of heat capacity and water content with Distributed Temperature Sensing (DTS) heated fiber optic systems presents an unprecedented opportunity for environmental monitoring. In this study we show that distributed measurements of soil volumetric heat capacity (Cs) and soil water content (θ) can be obtained by employing this approach. Here, we apply uniform heat pulses along a fiber optic cable and monitor the thermal response on an adjacent cable. We test the method using different combinations of fiber optic cables and heat sources at a range of spacings in a laboratory setting. The amplitude and phase-shift in the heat signal with distance was found to be a function of the soil heat capacity. Measurements of Cs from saturation to dry conditions were in the expected range, changing linearly with θ as described in the DPHP theory. Spatial variability measured within each cable at 0.125 m increments showed a coefficient of variation (CV) of 4 to 12 % independent of moisture content. Coefficients of variation for estimated Cs based on replicate measurements taken at saturation and dry conditions were 4 to 8 %.

Keywords: Fiber optic, dual probe, soil thermal properties, heat capacity, distributed measurement

1. Introduction

The magnitude of change of soil temperature in response to an energy input is controlled by the soil's heat capacity (C) and thermal conductivity (λ). Applications which aim to characterize soil heat interchange processes require, therefore, precise measurements of these soil thermal properties. Perhaps the most common application is to infer water content from measured thermal properties.

Soil heat capacity is defined as the quantity of heat required to change the temperature of a system per unit of mass. It can be reported as a specific heat capacity, c_s (KJ Kg $^{\circ}C^{-1}$), or volumetric heat capacity Cs (MJ m^{-3} $^{\circ}C^{-1}$), related via the soil bulk density. As soil systems are made up of diverse constituents—mineral, organic, water and air—the energy required to change the temperature of such system will depend on the proportion and nature of each of these constituents. In this sense it is common to express soil volumetric heat capacity as the weighted sum of the volumetric heat capacities of these components [de Vries, 1963]

$$C = \sum_{i=1}^{n} X_i \cdot C_i = \sum_{i=1}^{n} X_i \cdot \rho_i \cdot c_i \qquad (1)$$

Here X_i is the constituent volume fraction, and C_i represent the constituent volumetric heat capacity, c_i the specific heat capacity and ρ_i (Mg m^{-3}) the density of the n identified soil constituents. According to Kluitenberg [2002], a more practical expression is to express Eq. (1) using $X_i = \frac{(\emptyset_i \cdot \rho_b)}{\rho_i}$, where ϕ_i is the mass fraction, defined on a dry-mass basis, and ρ_i the density of each constituent. Including only the four major constituents previously discussed, Eq. 1 may be written:

$$C = \rho_b \cdot (c_o \cdot \emptyset_o + c_m \cdot \emptyset_m + c_w \cdot \theta g + c_a \emptyset_a) \qquad (2)$$

Where the subscripts "o", "m", "w" and "a" are organic, mineral, water and air, respectively, and θ_g is the gravimetric soil water content. Further simplifying by combining the mineral and organic fractions as the soil's solid phase with specific heat capacity, c_s, and by using θ as the volumetric soil water content, yields:

$$C = \rho_b \cdot c_s + \rho_b \cdot c_w \cdot \theta_g = \rho_b \cdot c_s + c_w \cdot \theta \quad (3)$$

This combined approach is in keeping with the specificity of the soil characterization typically available, and has been shown to provide good results, in part due to the fact that there is generally a modest variation of c_m and c_o among soils [Kluitenberg, 2002].

An alternative, direct, and non-destructive approach to measure soil heat capacity is the Dual Probe Heat Pulse (DPHP) method [Campbell et al., 1991; Bristow et al., 1993], generally implemented by inserting a pair of parallel needles separated by a distance r (measured center-to-center), in which the temperature response from heating one of the needles (via an electrical resistance) is obtained at the second needle (typically via a thermocouple). The DPHP interpretation employs the time and magnitude of the arrival of the maximum temperature at the thermocouple to derive soil volumetric heat capacity and soil thermal diffusivity. In a homogeneous, isothermal and isotropic porous medium, if an instantaneous heat pulse is applied to an infinite line source, the temperature rise at a distance r will be directly related to the amount of heat applied and inversely related to the volumetric heat of the medium [Carslaw and Jeager, 1959]

$$\Delta T(r,t) = Q(4\pi\alpha t)\exp\left(\frac{-r^2}{4\alpha t}\right) \quad (4)$$

Where ΔT is temperature (°C) rise from initial conditions, r is radial distance (m) at which the measurement is made, α is thermal diffusivity defined as the ratio λ/C ($m^2 s^{-1}$), and Q is the source strength (m^2 °C) which is defined as the heat input per unit of length, q (J m^{-1}) divided by the volumetric heat capacity of the medium ρc (J m^{-3} $^{\circ}C^{-1}$).

Setting the derivative of Eq. (4) with respect to time to zero one can directly solve for the maximum temperature increase at a fixed distance r to the line source, yielding $t_{max} = r^2/4\alpha$. Putting this result into Eq. (4) we obtain an expression for the maximum temperature rise as a function of the volumetric heat capacity.

$$\Delta T_{max} = \frac{Q}{e\pi r^2} = \frac{q}{e\pi r^2 \rho c} \tag{5}$$

Eq. (5) assumes that the heat is released instantaneously from the heater probe. To account for the finite duration of the heat release, a more recent model was provided by Knight and Kluitenberg [2004] which employs Eq. (5) together with a correction factor ε, defined as the ratio t_o/t_m, in which t_o is the duration of the heat pulse and t_m is the elapsed time from the beginning of the heat pulse to the occurrence of the maximum temperature rise.

$$C = \frac{q}{e\pi r^2 \Delta T_{max}} \left| 1 - \frac{\varepsilon^2}{8} \left\{ \frac{1}{3} + \varepsilon \left[\frac{1}{3} + \frac{\varepsilon}{8} \left(\frac{5}{2} + \frac{7\varepsilon}{3} \right) \right] \right\} \right| \tag{6}$$

DPHP sensors do not meet the idealized geometry and heating characteristics embodied in the infinite line solution. Rather, they have non-zero radii, finite length and heat capacity differing from that of the soil. These aspects call into question the accuracy of such devices when employing Eq. (5), however, as discussed in Kluitenberg et al. [1993], the error in estimated values of C in comparison with models using more precise geometric

descriptions [de Vries, 1952; Carslaw and Jeager, 1959] has been found to be on the order of 1%.

A major source of uncertainty in all kind of DPHP models is assigning the appropriate value of the radial distance (r). Campbell et al., [1991] and Ham and Benson [2004] point out that a 2% error in r will lead to a 4% error in C. The matter of physically establishing a prescribed probe spacing, and the value of r that best represents that geometry, is a fundamental issue to be addressed. A common approach to account for the probe finite dimensions is to calibrate for the apparent probe spacing (r_{app}) [Tarara and Ham, 1997; Song et al., 1998; Bristow et al., 2001; Basinger et al., 2003; Ochsner et al., 2003; Kinight and Kluitenberg, 2012]. An experimental approach can be used, for instance, if the sensors can be immersed in mediums of known properties, such as water immobilized with agar, to interfere r from Eq. (5) as the apparent probe spacing . Once r_{app} is defined, spatial attention must be paid when inserting the needles into the soil since deflection might occur due to the reduced probe thickness.

Due to the strong dependence of C with water content in porous media [e.g., de Vries, 1963] DPHP can also be used to estimate soil moisture by measuring basic soil properties such as the soil bulk density and using published values of most common soils´ specific heat capacities [Campbell, 1991; Tarara et al., 1997; Song et al., 1998; Kluitenberg, 2002].

Although the theory of DPHP is well established and proven in a wide range of settings, a major limitation is that it has thus far been implemented as a point measurement, and thus is difficult to employ in characterizing dynamic patterns of spatial variability. To obtain accurate measurements of soil thermal properties at scales which represent fields or

watersheds (1 to 1,000 m) would require an enormous number of measurements and repetitions. In practice such repeated measurements with an inserted probe would be laborious, would include "nugget" effect variations in readings (in the sense of a variogram), and would be susceptible to systematic errors due to probe wear and deflection during insertion.

An approach to allow DPHP to span larger spatial scales and to eliminate errors due to re-insertion of a probe would be the use of a device composed of a line source as a heat emitter and very large number of thermal sensors mounted in parallel. This scenario can be approximated by using fiber optics and a Distributed Temperature Sensing equipment. Current DTS equipment can achieve 0.29 m spatial and 1 s temporal resolution, and provide this along cables of kilometers in length. An advantage of the DTS over the usual DPHP approach is that fibers can be included in both the heater and the passive observation cable. That is to say, it is equivalent to having a thermocouple in both the heated and observation probes of a DPHP system.

Though relatively recently finding broad-scale adoption, over the last decade fiber optics DTS systems have been employed to obtain distributed temperature measurements in a spectrum of hydrological and environmental applications [e.g., Selker et al., 2006a, 2006b; Westhoff et al., 2007; Freifeld et al., 2008; Tyler et al., 2008, 2009; Steele-Dunne et al., 2010; Vercauteren et al., 2011; Thomas et al., 2012]. In addition to these applications where the cable was employed to measure the temperature of its surroundings, fiber optics DTS can also be used to analyze the thermal characteristics of the environment surrounding the cable in the so called Active Heated Fiber Optics method (AHFO). Here, heat is uniformly applied by electrical resistance to the stainless steel armoring jacket or an added

conductor symmetrically positioned (wrapped) about the fiber optic cable. It is basically an application of the classical single probe theory in which the heat source and the thermal sensor are mounted in the same fiber optic cable [De Vries et al., 1958; Kluitenberg et al., 1993; Bristow et al., 1994]. Main applications of the AHFO methods are the estimation of soil thermal conductivity [Weiss, 2003; Ciocca et al., 2012], water movement trough the porous medium [Aufleger et al., 2005; Perzlmaier 2004, 2006] or the estimation of soil water content [Weiss, 2003; Sayde et al., 2010; Gil et al., 2012; Sayde et al., 2012]

Although single cable AHFO applications to monitor SWC are promising, further research to address the fundamental issue of large scale calibration is still required. While application in homogenous conditions can be implemented through calibration routines previously defined in the laboratory, its use in heterogeneous soil conditions remain challenging. The use of heated fiber optic as proposed in this study is expected to minimize such calibration problems since the method is based on the linearity of the response to change in heat capacity due to change in water content.

The objective of this manuscript is to test the feasibility of heated fiber optics to estimate soil volumetric heat capacity and soil volumetric water content as described in the classic DPHP theory [Campbell et al., 1991; Bristow et al., 1993]. Here, we present an AHFO set up in which several fiber optic cables of different diameters and with various protective sheathings were located in parallel in a long plastic box filled with loamy sand. We created different combinations of cables and spacings by applying electricity to one of the cables (heat emitter), and then monitor the thermal response at the cables collocated on both sides (thermal sensors). The feasibility of the method was tested from saturation to dry conditions against soil moisture and thermal sensors installed at the depth of the cables.

2. Materials and methods

2.1 Experimental set up

The experiment was built in the laboratory using a methacrylate box of 2.5 m x 0.25 m x 0.25 m which was placed in an open-top flume channel (Fig. 1). The bottom was uniformly perforated with 4 mm holes on 0.01 m spacing, which was covered with two overlapped 1 mm opening mesh to allow for free drainage. Openings at the front and the rear of the box provided entries for the cables, while four openings at the wall allowed the insertion of soil moisture sensors (Fig. 2).

Three different types of fiber optic cable were used in the experiment. Two cables had centrally located hermetically sealed stainless steel tubes encasing the fiber optics. The larger of the two had a 3.8 mm diameter nylon jacket covering a layer of helically wrapped of stainless steel strands about the 1.35 mm outer stainless tube ("Brusteel," Brugg Cable, Brugg, Switzerland). The second stainless-tube cable had a 2 mm PVDF jacket over its 1.20 mm outer stainless tube (custom made by AFL, USA). The third cable had no steel elements, consisting of a simple 1-mm plastic tube enclosing Corning Clear Curve fiber (Corning incorporated, USA) (Table 1; Fig. 3). Hereafter these cable constructions are referred to as $FO_{3.8mm}$, FO_{2mm}, and FO_{1mm}. Each type of cable traversed the box twice, resulting in six passes of fiber optic cable, each of 2.5 m length. All were employed in the analysis, and the cables in the soil are referred to as $FO_{1mm\text{-}A}$, $FO_{1mm\text{-}B}$, $FO_{2mm\text{-}A}$, $FO_{2mm\text{-}B}$, $FO_{3.8mm\text{-}A}$ and $FO_{3.8mm\text{-}B}$, (Figs. 2 and 3). The fibers were fusion-spliced into a single optical path creating a double ended configuration (e.g., van de Giesen et al., 2012). The total length of the optical path was 95 m, of which 15 m was within the box. The other 80 m were reserved for calibration, routing, or attachment of power for heating (Fig. 2).

The spacing and positioning of the cables within the box was achieved by using two sets of spacers: a primary group was anchored to the box, ensuring both fiber spacing and positioning (Fig. 1), and a secondary much smaller spacer design was included purely to control cable spacing (Fig. 3). In the first group, 4 methacrylate rectangular plates, 0.25 m depth and 0.1 m wide, were placed perpendicular to the box´s longitudinal axis at a distance of 0.3, 0.8, 1.35 and 1.90 m, respectively, to the beginning of the box. These permanent spacer plates were co-aligned with the perpendicular bisector of the box´s width by screwing their upper part to a wooden post, anchored at the same time to the lateral walls of the box, which ensured stability and perpendicularity. Fine-tuning of the cable alignment was achieved by leaving 0.01 m of clearance between the wooden post and the spacer plate by using different drilling diameters i.e. once they were screwed, the spacer plate had a relative freedom of movement in the vertical plane perpendicular to the longitudinal axis of the box (Fig. 1). The positioning of the fiber within the box was controlled by passing the cables through three blocks with precisely-located holes drilled to just pass the three sizes of cables (Fig. 1). The smaller spacers employed consisted on 16 methacrylate plates, 0.01 m depth and 0.03 m wide, which were able to move along the cables, designed solely to maintain the cable spacing.

Once the cables were emplaced, they needed to be drawn tight to provide for consistent placement between spacers. Four stainless steel wedge clamps held the 3.8 and 2 mm cables securely but without impingements allowing the imposition of tension on the cables (Fig. 1). As FO_{1mm} did not include an armoring steel tube, and therefore was more susceptible to impingements and fiber breakage due to tensile stress, a second stretching tool was designed specifically for this cable.

The box was filled with a sandy loamy soil, which had been passed through a 2 mm sieve, in lifts of 0.05 m. Each lift was settled with continuous vibrations by tapping a rubber mallet on the walls of the box. The filling process was carried out in three steps: a first step to fill up the box until the cables depth, a second step to install the sensors and finish the cables stretching and, finally, a third step to complete the total filling. Three $1 \cdot 10^{-4}$ m^3 m^{-3} soil samples of the media were taken to determine in-situ bulk density, yielding values of 1.47, 1.58, and 1.48 kg m^{-3}, with a mean value of 1.51 kg m^{-3}.

The DTS unit employed was a Silixa Ultima SR (Silixa Ltd, UK) set to sample on 0.125 m increments, and which has spatial and temporal resolution of 0.29 m and 1 s. However, as the cable deployment followed a double-ended set up, the acquisition frequency was 2-3 s depending on the DTS ability to alternately process the data from each of two channels. Effects of differential attenuation, fusion splices and any irregularities in fiber optical properties were calibrated for using the internal calibration routine provided by the DTS manufacturer, which with the double ended set up allowed for correction of spatially varying attenuation. Two PT-100 temperature probes, recording directly to the DTS, were placed in the reference temperature bath. As expected for such a short optical path, no offsets or differential attenuation were observed.

Soil water content in the vicinity of the cables was monitored with four soil moisture sensors (5TM Echo probe, Decagon, USA) which were installed 0.43, 0.95, 1.50, and 2.00 m from one end of the box (referred to as Echo 1, 3, 4 and 5). The Echo probes were placed at the depth of the cables during filling and buried with the cables. An additional Echo probe (Echo 2) was placed in parallel to, but 0.03 m above, Echo 1 to provide a redundant measurement. Unfortunately, after 35 days Echo probes 2 and 4 failed for unknown

reasons. Soil thermal properties were monitored with a thermal probe analyzer (KD2pro, Decagon, USA) which was placed in the same manner as the Echo probes 0.03 m above the cables and attached to the second plate spacer (Fig. 2).

Uniform heating of the cables was obtained by passing electrical current along the stainless steel armoring jacket of a sections of 4.8 m, 4.45 m and 4.3 m of $FO_{3.8mm\text{-}A}$, $FO_{2mm\text{-}A}$ and $FO_{2mm\text{-}B}$, respectively, following the approach of Sayde et al. [2010]. Power was supplied from a 220V AC building circuit, with a voltage regulator employed to provide specific, constant power levels (Fig. 2). Heat pulses designed to deliver 40 W m^{-1} with 40 s duration were used with the $FO_{3.8mm}$, and 32 W m^{-1}, and 45 s with the FO_{2mm}. These prescribed power rates were sought to be sufficient to provide a 1.5 °C temperature rise at the cables adjacent to the heat source when the soil was at a saturated condition i.e. for a DTS reported accuracy of 0.3 °C, we sought a maximum temperature increase five times larger than the expected error. Minor variations in the power intensity resulted primarily from a systematic increase in resistance of the stainless steel as its temperature increased, as well as minor variations in the voltage of the power mains. A power meter was employed to document actual heat delivery (PCE-PCM1, PCE Ibérica, Spain) at 50 to 200 Hz frequency (Fig. 2).

2.2 Determination of soil volumetric heat capacity

Using Eq. (6), the variables required to be measured were q, r, t_m, and ΔT_{max}. Precise spacing between cables was obtained in the box filling process, and verified with a 0.01 mm precision dial caliper (Table 2). However, in order to be consistent with Eq. (6), r must consider the distance between geometrical centers of the cables and, additional to the

mentioned soil spacing, it must include the thickness of the protective sheathings. When these materials are included into the system, the C computed value is no longer exclusively influenced by the surrounding soil, but rather it is also affected by these materials. To account for these non-soil constituents we employed an approximate representation of the system geometries in which the computed C value using Eq. (6) was taken to be proportional to the weighted sum of the volumetric fractions and volumetric heat capacities of the different constituents in the system i.e. surrounding soil, filling gel, stainless steel, nylon, PVC, and PVDF (Table 2). We sought a rational, readily applied approach to defining the system. The Volumetric fractions were approximated to the ratio of the area occupied for each specific constituent over the total area defined as the interior tangent circumference to the two corresponding cables. For example, in the case of two $FO_{3.8mm}$ cables (Fig. 4), C is calculated as

$$C = X_S \cdot C_S + X_{FG} \cdot C_{FG} + X_{SST} \cdot C_{SST} + X_N \cdot C_N \quad (7)$$

In which C is the computed volumetric heat capacity accordingly to (6), X is the volumetric fraction, and the subscripts, "$_S$" "$_{FG}$", "$_{SST}$" and "$_N$" are soil, filling gel, stainless steel and nylon (or more broadly, the jacket material), respectively. The rest of combinations were calculated following the same procedure.

ΔT_{max} was defined as the DTS reported maximum temperature increase over a temperature baseline defined as the 2 min average DTS reading previous to the heat pulse (Fig. 5). T_{max} was defined using the average value of the three highest temperature readings of the heat pulse which also defined the average time of occurrence t_m. Besides saturation were the DTS signal to noise ratio was more pronounced, the three highest temperature readings

occurred in all cases within ± 10s. In general, the definition of ΔT_{max} should be a function of the duration of the heat pulse (it must be considerably shorter than this parameter), the temporal resolution of the DTS (it should be longer than this parameter), and the signal to noise ratio between the computed ΔT_{max} and the performance of the DTS. In the case of signal to noise, the averaging period over which ΔT_{max} is computed should be selected so as to allow differentiation (in a statistical sense) of successive values of ΔT_{max}. We have selected ΔT_{max} operationally here using a practicable value, but clearly this is an area where further development would be required to optimize the performance of DTS-based DPHP methodology, which is likely to make the optimal value of ΔT_{max} a function of the cable, the DTS, the soil, and even the particular soil-water status.

Since FO cables at the entrance and exit of the box could be influenced by partial exposition to the air (the DTS has 0.29 m resolution), the first 0.45 m of cable at both extremes of the box were excluded for data analysis and the available length of measurement was reduced to approximately 1.8 m.

Saturation and drainage were obtained by controlling the water level in the flume. It must be noted that the soil was unexpectedly affected by shrinking, with a few soil cracks appearing after the first 15 days of free drainage. This effect was most pronounced at the first 0.3 m of each end of the box, while in the rest of the box the soil only cracked at the walls and at the spacer plates (Fig. 6). As measurements within 0.30 m of the ends of the box were not included in the analysis, the cracking did not appear to have influenced the reported measurement area.

3. Results and Discussion

3.1 Determination of volumetric heat capacity by the dual probe method

As the soil in the experimental box dried out, nine measurements at known θ were collected, including a first measurement in saturation; observations through the use of moisture probes and three $1 \cdot 10^{-4}$ m^3 soil samples in saturation—mean value from n=3 samples, $\theta_{sat} = 0.32$ m^3 m^{-3}. In each measurement, three heat pulses sequentially distributed every 30 min to $FO_{3.8mm\text{-}A}$, $FO_{2mm\text{-}A}$ and $FO_{2mm\text{-}B}$ were applied. Since each heated source had two adjacent FO cables, in total, three C_s pairs of heating/observation data were obtained per measurement i.e. two reading per heated cable (Table 3). For a DTS sampling resolution of 0.125 m between 14 to 15 points per cable were analyzed, depending on the apparent influence of the boundary condition effect i.e. the influence of the partially air-exposed section of the cable to the contiguous points. It must be noted that although measurements at 0.125 m increments are not independent in a thermal sense—the actual DTS spatial resolution is 0.29 m—they are independent to the instrument noise, and thus provide independent values from the standpoint of statistical noise intrinsic to the measurement method.

The coefficient of variation (CV) of Cs measurements at each cable was found to be 4 to 12 %, with no apparent relationship between uncertainty and the value of θ (Table 3; Fig. 7). Considering the soil to be homogeneous, this variability would be expected to have come from: non-uniform drying throughout the box—assumed to be similar to variations detected through installed moisture probes (Table 4); deviations in probe spacing—expected to be minimum due to the effect of the spacers and stretching clamps—and; the intrinsically DTS uncertainty to measure ΔT_{max} in Eq. (6). In order to quantify DTS uncertainty, we analyze

the precision of the DTS measurements through repetitions at dry (θ=0.09 m^3 m^{-3}) and saturated (θ=0.32 m^3 m^{-3}) conditions (Table 5). The average CV obtained from the 14-15 point within each cable shows a precision of about 4 to 8% with higher CV at greater levels of saturation. This might be explained by the value of ΔT_{max} (inverse with θ) relative to the DTS noise (constant with θ), therefore estimation of moisture content based on ΔT_{max} would be expected to have greater relative measurement error at higher moisture contents. It must be noted that better precision might have been achieved by employing a power controller device to minimize variations in the total power applied due to variations in the electrical main, employing a higher performance DTS system (or different settings of the DTS, such as single-ended measurements, which would have doubled the effective frequency of measurement), using higher power levels, or different heat pulses. Further, we have used the raw data rather than fitting an analytical model to the data and then computing the apparent ΔT_{max}. In our case we are basing the entire computation on a few data points, whereas a fit model of the data would be able to employ the entire data set. Clearly there is great opportunity to further optimize this technique and gain better precision, but this will be the basis for future work, whereas this study had the objective of proof-of-concept, for which the direct analysis employed resulted in the most transparent outcome.

3.2 Calibration for the apparent radial distance

In order to account for the finite dimensions of the probe, a common approach in the DPHP method is to calibrate the radial distance in a medium of controlled volumetric heat capacity. Here, we employed measurements with the thermal probe as a reference values.

Results from the buried thermal probe found Cs ranging from 2.47 MJ m^{-3} $°C^{-1}$ at saturation to 1.28 MJ m^{-3} $°C^{-1}$ at dry conditions and which suggest a faster and more complete drying at these probes relative to the DTS values obtained through calculation of Eq. (6) (i.e. measurements from the KD2Pro probes remain stable at dry conditions beyond the 5th measurement, Table 3). Recalling that these probes were directly attached to the spacer plates, we think it is likely that these features arose from the influence of the aforementioned soil cracks which would be expected to have enhanced drying in the vicinity of the probes. Although these intermediate soil moisture results cannot be then employed to test the accuracy of the method, we think they are acceptable to be employed to quantify the range of Cs from saturation to dry conditions, and as reference Cs value at saturation. Although Cs variability decreased at lower values of θs, we have more confidence in the data at saturation where the controlled water level in the flume canal minimized θ heterogeneity.

Using r in Eq. (6) as a calibration parameter—apparent probe spacing (r_{app}), Cs can be matched to the thermal probe Cs reference value at saturation (approximately 2.50 MJ m^{-3} $°C^{-1}$). Table 2 shows r_{app} for each cable and Fig. 8 Cs values after calibration. The resulting fitted equation in Fig. 8—results obtained by averring Cs mean values after calibration—showed a slope of 5.98 MJ m^{-3} $°C^{-1}$with a standard deviation of 0.19 MJ m^{-3} $°C^{-1}$, an intercept of 0.60 MJ m^{-3} $°C^{-1}$, and R^2=0.99. This results show a linear relationship between Cs-θ with a slope larger than expected i.e. 4.186 MJ m^{-3} $°C^{-1}$ using the volumetric heat capacity of water at 20 °C in Eq. (3).

Overestimations on the slope of the Cs-θ relationship is expected to impose larger error in θ measurements with decreasing soil water content. A linear regression analysis using

average values from Echo 1, 3 and 5 confirmed this statement showing underestimations of θ through calculation of Eq. (3) with increasing differences as the soil dried out (Fig. 9). Increased bias with decreasing soil water content has been reported before when the apparent probe spacing is calibrated at saturation in the DPHP method (Tarara and Ham, 1997; Song et al., 1998; Bristow et al., 2001; Basinger et al., 2003; Ochsner et al., 2003). According to Kinight and Kluitenberg (2012) deviations in Cs estimates are attributed to the probe finite dimensions and the dependence of the apparent spacing on the heat capacity of the calibration medium. This study is primarily focused on proof of concept, so here we seek to illustrate that DTS cable systems can be calibrated via adjustment of the parameters included in the model, though optimization of calibration will require further study in diverse soils.

Other sources of uncertainty are related to the considerable thermal influence of the jacketing material and the not inconsiderable uncertainty of the reference Echo soil moisture probes. Considering that two out of five moisture probes failed during the experiment, we suggest further research to address the reliability of these devices in the proximity of high-current electrical circuits due to interferences due to induction and linear elements of high electrical conductivity

3.3 Conclusions

The feasibility of using heated fiber optics with distributed temperature sensing to obtain soil volumetric heat capacity has been demonstrated in this study. From the combinations of geometries, heat sources and protective materials employed, results have confirmed the ability of the method to successfully implement the DPHP methodology to this system.

Although Cs measurements using FO_{1mm-B} required calibration, the majority fall within the expected range of parameter values (Cs), with the usual linear relationship to θ. Observed deviations from the expected slope using eq.(3) were attributed to the intrinsic use of finite dimensions probes and the previously reported dependency of r_{app} with θ.

Limitations of the method were attributable to the DTS signal to noise ratio and the accuracy of detecting a peak in the temporal signal (T_{max}). This led to a +/- 4 to 8 % uncertainty in Cs through repetitions at dry and saturated conditions. Cs uncertainty during the experiment increased up 12% as non-homogenous dry out enhanced spatial variability throughout the box. Nevertheless, better results are expected as improvements in DTS accuracy are achieved.

The feasibility of the method to calculate θ as described in the classic DPHP and through the use of Eq. (3) has been shown, though results were undermined by observed deviations in the slope of the relationship of Cs to θ which imposed larger error in θ estimations with decreasing water content. Other sources of uncertainty were attributed to the thermal influence of the jacketing material and the own uncertainty of the reference moisture probes. In this regard, further research to address the most suitable reference method for independent moisture measurement in the context of AHFO is required.

Further opportunities to improve the method should include (i) more sophisticate calibration methods to effectively address the geometry of cable and the influence of the jacketing material ; (ii) new strategies to optimize the duration and intensity of the heat pulses including effective targeting criteria for ΔT_{max} estimations; (iii) the use of analytical-

based models to include the entire data set and to improve the precision of the DTS reported ΔT_{max}.

While these laboratory results suggest that the potential for application under field operation conditions are encouraging, many challenges remain, prominently including deployment of the cable which assures consistency of probe spacing under the diversity of soil conditions which should be expected (e.g., where stones and swelling constituents are often present). In this regard, fiber optic and cable burial manufactures will have an important role in improving the method, including also new opportunities for optimization of the cable design. We expect that widespread installation would require a cable which has a two-dimensional geometry that maintains exact spacing between source and sensing elements.

Acknowledgements

The authors would like to thank Raúl Sánchez, Javier Granja and Juan Carlos Garrido for their very helpful support. We also acknowledge the inter-ministerial commission of Science and Technology (CICYT) for their support at the project AGL2004-01689 and the Center for Transformative Environmental Monitoring Programs (CTEMPS.org, NSF grant # 1129003) for their technical support.

Fig. 1. The experimental chamber in the flume before being filled with soil. The four spacer plates are seen, as well as the smaller blocks holding the white cables at proper spacing

Fig. 2. Conceptual sketch of the fiber optic installation focusing on heating and calibration.

Fig. 3. Detail of the 6 fiber optic cables. Also detail of the second kind of spacers. Only FO2mm-A , FO2mm-B, FO3.8mm-A are used as heaters.

Fig. 4. Example of the system in the case of two FO3.8mm cables. The volumetric fractions are substituted for surface proportions. In this case T, N, STT and FG which are the subscripts for Total, Nylon, Stainless steel and Filling gel. The largest circle is the interior tangent circumference to the FO3.8mm cables and represents the total area. Soil separation is 1, and probe spacing is 2.

Fig. 5. DTS captured thermal response at FO2mm-B to a 45 s 32 W m-1 heat pulse of and the subsequent 500 s period during cool dawn.

Fig. 6. Detail of observed soil cracks after 80 days of experiment at different sections in the box. Bottom right shows a detail of the second spacer plate where the thermal probe was installed (white cable)

Fig. 7. Coefficient of Variation (C.V) as a function of soil water content for the different cables employed. The values are obtained from n=14-15 points per cable

Fig. 8. Mean Cs values after calibration (14-15 points per cable) as θ varies (observations through average readings from probes Echo 1, 3 and 5). Calculated trend (solid line)) from average Cs calibrated values. Also, expected trend according to Eq. (3) (dashed line)

Fig. 9. Linear regression between calculated θ (DTS measurements using Eq. (3)) and measured θ (average from Echo 1, 3 and 5). R2= 0.99 with y = 0.6844x + 0.0811.

Table 1. Summary of the main geometrical and physical characteristics of the different types of fiber optics employed in the experiment

Manufacturer	**Diameter**	**Materials**	**Thickness**	**C**	**Source of thermal properties**
	mm		*mm*	$MJ\ m^{-3}\ K^{-1}$	
Brugg	3.8	Filling gel & fiber	0.55	1.6	Manufacturer
		Stainless steel tube & Stainless stranded elements	0.5	3.8	Peckner and Bernstein [1977]
		Nylon Jacket	0.825	2.2	Manufacturer
AFL	2.0	Filling gel & fiber	0.475	1.6	Manufacturer
		Stainless steel tube	0.125	3.8	Peckner and Bernstein [1977]
		PVDF	0.4	2.1	Kok et al., [2008]
Corning Clear Curve LBL	1.0	Fiber cladding	0.3125	1.6	Manufacturer
		PVC	0.1875	1.4	Kok et al., [2008]

Table 2. Summary of the geometric properties of fiber optic cable combinations employed here. Soil spacing indicates the distance between outer surfaces (from the heated cable to the adjacent observation cable) and probe spacing the distance between geometrical centers.

Heated cable	**Observation cable**		**Soil spacing**		**Probe spacing**		**Apparent probe spacing (r_{app})**	
	Left	Right	Left	Right	Left	Right	Left	Right
			mm					
FO_{2mm-A}	FO_{1mm-A}	FO_{2mm-B}	5.96	3.95	7.41	5.95	7.20	6.10
FO_{2mm-B}	FO_{2mm-A}	FO_{1mm-B}	3.95	3.85	5.95	5.30	5.85	6.10
$FO_{3.8mm-A}$	FO_{1mm-B}	$FO_{3.8mm-B}$	3.96	4.40	6.31	8.20	7.15	8.10

Table 3. C_s (means and standard deviations in brackets) as computed from DTS data at each cable for 9 observations over the 81 days of experiment. Average θ and C obtained from the moisture and thermal probes are presented for reference.

	Heated source		**FO_{2mm-B}**		**FO_{2mm-A}**		**$FO_{3.8mm-A}$**	
	Thermistor		**FO_{1mm-B}**	**FO_{2mm-A}**	**FO_{1mm-A}**	**FO_{2mm-B}**	**FO_{1mm-B}**	**$FO_{3.8mm-B}$**
day	**KD2pro**	**θ^***	**C_s^{**}**					
	$MJ\ m^{-3}\ ^oC^{-1}$	*$m^3\ m^{-3}$*	----------*$MJ\ m^{-3}\ ^oC^{-1}$*----------					
0	2.47	0.32	3.42(0.24)	2.67(0.10)	2.35(0.17)	2.68(0.22)	3.32(0.35)	2.38(0.14)
20	1.86	0.22	2.54(0.10)	2.07(0.12)	1.72(0.17)	2.02(0.13)	2.53(0.22)	1.93(0.17)
24	1.55	0.20	2.52(0.20)	1.98(0.08)	1.7(0.13)	1.86(0.11)	2.34(0.19)	1.79(0.14)
32	1.31	0.17	2.33(0.13)	1.72(0.21)	1.57(0.11)	1.69(0.15)	2.19(0.15)	1.63(0.12)
35	1.29	0.15	1.99(0.14)	1.54(0.11)	1.40(0.09)	1.52(0.10)	2.19(0.22)	1.42(0.07)
42	1.26	0.13	1.81(0.15)	1.44(0.17)	1.18(0.12)	1.31(0.11)	1.79(0.16)	1.35(0.11)
53	1.28	0.11	1.66(0.12)	1.36(0.07)	1.26(0.14)	1.29(0.09)	1.64(0.09)	1.19(0.05)
62	1.28	0.10	1.67(0.07)	1.27(0.10)	1.22(0.11)	1.20(0.10)	1.61(0.11)	1.18(0.08)
81	1.28	0.09	1.52(0.08)	1.23(0.09)	1.12(0.07)	1.17(0.09)	1.57(0.13)	1.12(0.09)

* Moisture probe measurements

**Average Cs and standard deviation in 0.125 m increments (14-15 points per cable)

Table 4. Summary of θ observations by the soil moisture probes. Dashes indicate failed sensors.

day	Echo 1	Echo 2	Echo 3	Echo 4	Echo 5	mean*	C.V*
	---------- $m^3\ m^{-3}$ ----------						%
0	0.312	0.286	0.317	0.354	0.319	0.316	1.2
20	0.228	0.230	0.217	0.238	0.220	0.221	2.5
24	0.201	0.202	0.192	0.207	0.195	0.196	2.5
32	0.174	-	0.162	0.152	0.160	0.165	4.7
35	0.164	-	0.141	-	0.143	0.149	8.4
42	0.144	-	0.119	-	0.119	0.128	11.5
53	0.132	-	0.097	-	0.102	0.110	17.3
62	0.117	-	0.087	-	0.091	0.098	16.8
81	0.105	-	0.085	-	0.087	0.092	11.6

* Measurements from echo 1, 2 and 3

Table 5. Analysis of repeatability of DTS measurements at dry and saturated conditions.

		Dry*		Saturated*	
Heated source	**Thermal sensor**	**Cs****	**CV**	**Cs****	**CV**
		$MJ\,m^{-3}\,{}^{o}C^{-1}$	%	$MJ\,m^{-3}\,{}^{o}C^{-1}$	%
$FO_{2mm\text{-}B}$	$FO_{1mm\text{-}B}$	1.51(0.07)	4.3	3.43(0.20)	5.8
	$FO_{2mm\text{-}A}$	1.23(0.05)	4.0	2.68(0.17)	6.3
$FO_{2mm\text{-}A}$	$FO_{1mm\text{-}A}$	1.12(0.05)	4.2	2.21(0.16)	7.2
	$FO_{2mm\text{-}B}$	1.17(0.06)	5.2	2.64(0.18)	7.0
$FO_{3.8mm\text{-}A}$	$FO_{1mm\text{-}B}$	1.56(0.06)	4.1	3.10(0.14)	4.6
	$FO_{3.8mm\text{-}B}$	1.11(0.07)	6.2	2.37(0.19)	8.0

*Measurements from three repetitions

**Means and standard deviations over 14-15 points per cable

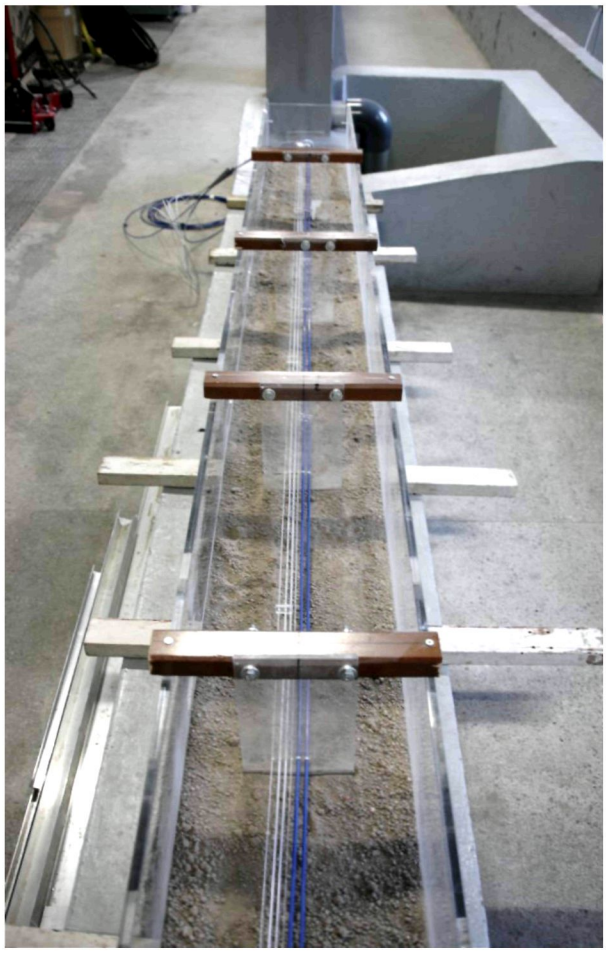

Fig. 1. The experimental chamber in the flume before being filled with soil. The four spacer plates are seen, as well as the smaller blocks holding the white cables at proper spacing.

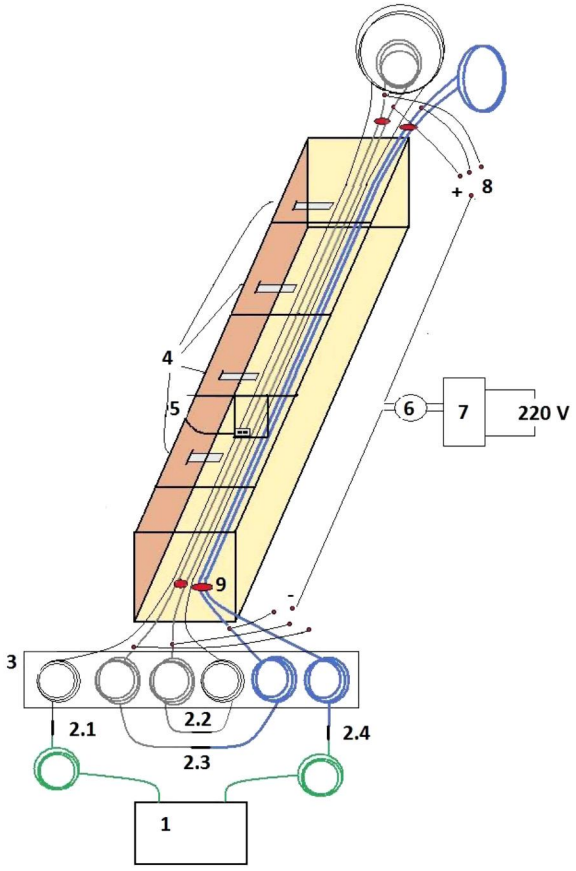

1. DTS
2.1. Fusion splice DTS- FO_{1mm}
2.2. Fusion splice FO_{1mm}- FO_{2mm}
2.3. Fusion splice FO_{2mm}- $FO_{3.8mm}$
2.4. Fusion Splice $FO_{3.8mm}$-DTS
3. Calibration bath
4. Moisture probe
5.Thermal probe
6.Wattmeter
7.Voltage regulator
8.Electrical.conenctions
9.Stretching clamps

Fig. 2. Conceptual sketch of the fiber optic installation focusing on heating and calibration.

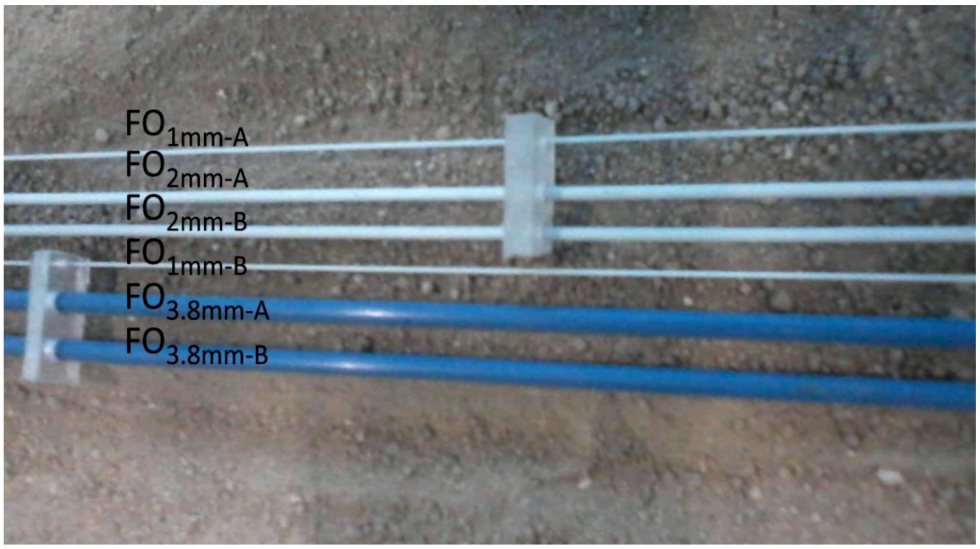

Fig. 3. Detail of the 6 fiber optic cables. Also detail of the second kind of spacers. Only $FO_{2mm\text{-}A}$, $FO_{2mm\text{-}B}$, $FO_{3.8mm\text{-}A}$ are used as heaters.

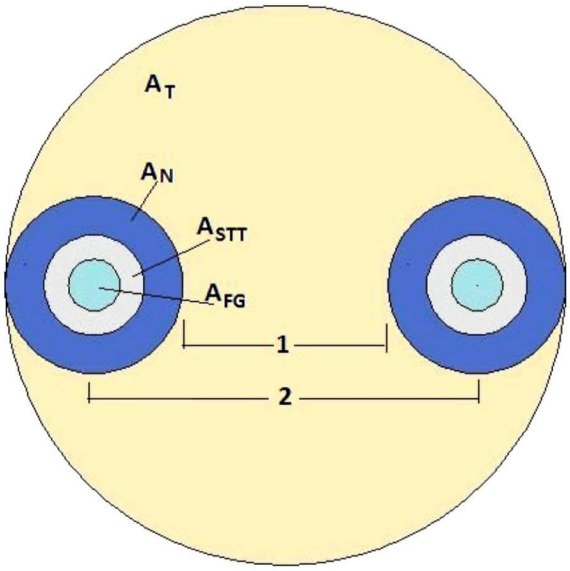

Fig. 4. Example of the system in the case of two $FO_{3.8mm}$ cables. The volumetric fractions are substituted for surface proportions. In this case T, N, STT and FG which are the subscripts for Total, Nylon, Stainless steel and Filling gel. The largest circle is the interior tangent circumference to the $FO_{3.8mm}$ cables and represents the total area. Soil separation is 1, and probe spacing is 2.

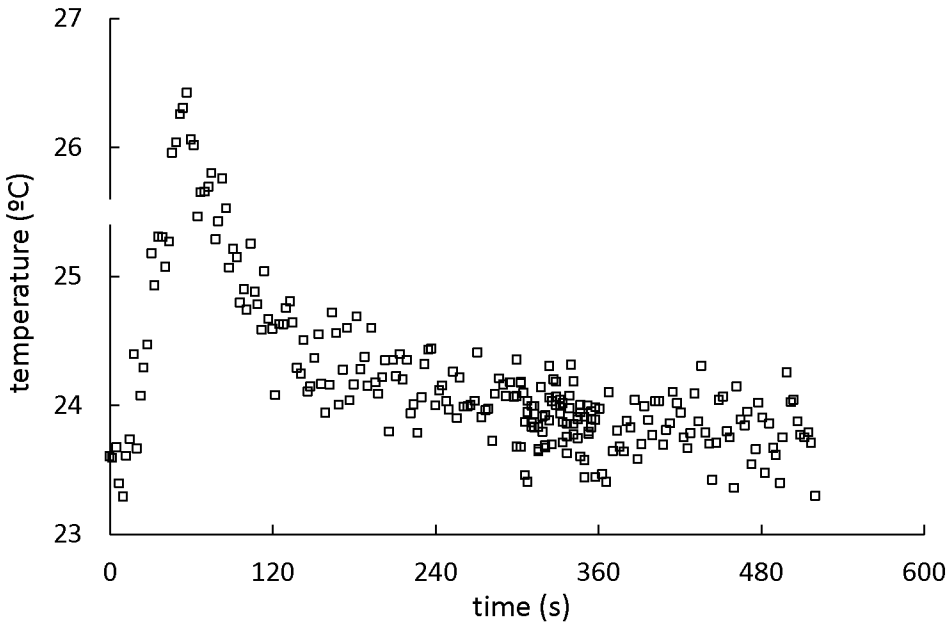

Fig. 5. DTS captured thermal response at FO_{2mm-B} to a 45 s 32 W m^{-1} heat pulse of and the subsequent 500 s period during cool dawn.

Fig. 6. Detail of observed soil cracks after 80 days of experiment at different sections in the box. Bottom right shows a detail of the second spacer plate where the thermal probe was installed (white cable)

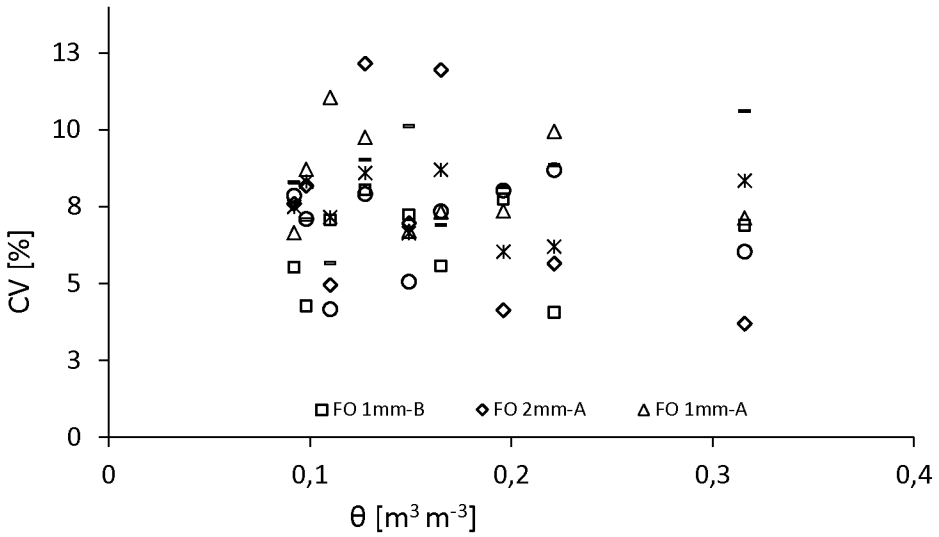

Fig. 7. Coefficient of Variation (C.V) as a function of soil water content for the different cables employed. The values are obtained from n=14-15 points per cable

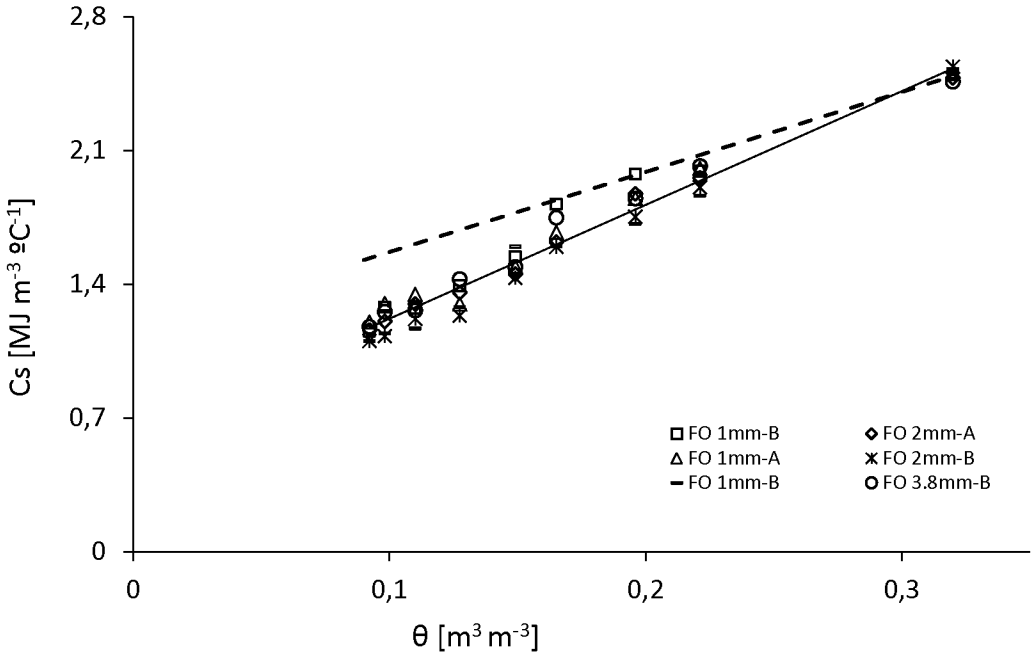

Fig. 8. Mean Cs values after calibration (14-15 points per cable) as θ varies (observations through average readings from probes Echo 1, 3 and 5). Calculated trend (solid line)) from average Cs calibrated values. Also, expected trend according to Eq. (3) (dashed line)

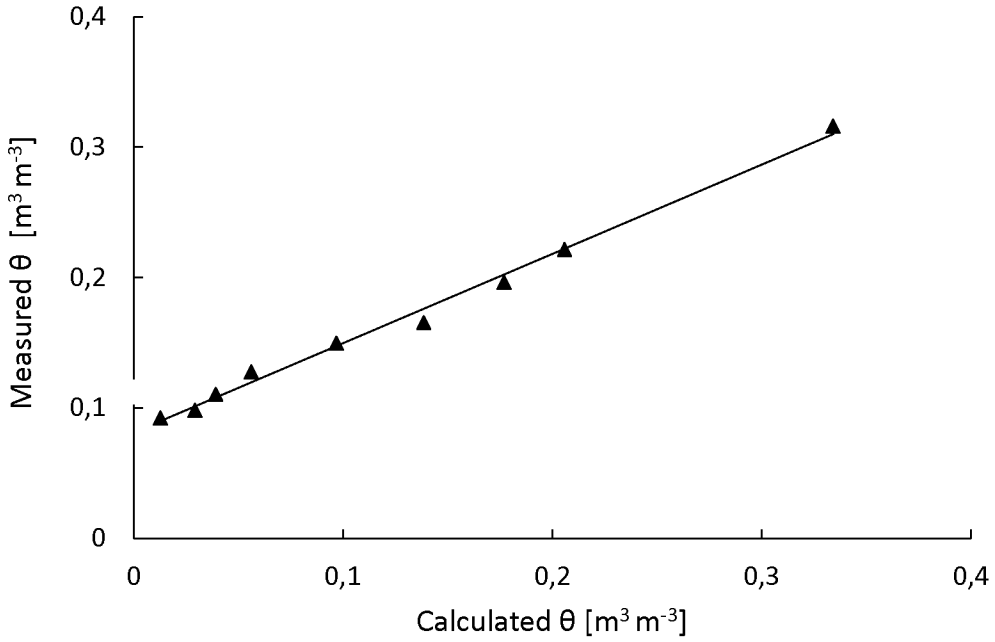

Fig. 9. Fig. 9. Linear regression between calculated θ (DTS measurements using Eq. (3)) and measured θ (average from Echo 1, 3 and 5). R^2= 0.99 with y = 0.6844x + 0.0811.